ACS Catalysis

pubs.acs.org/acscatalysis Research Article

A Unified Mechanism Reveals the Evolutionary Origin of Enoyl Isomerases

Bing Chen,[#] Jinwei Ren,[#] Huimin Zhao,[*] and Bin Wang[*]

Cite This: *ACS Catal.* 2025, 15, 15649−15656 Read Online

ACCESS | Metrics & More | Article Recommendations | Supporting Information

ABSTRACT: Enoyl isomerases (EIs) and dehydratases (DHs) are critical for diversifying polyketide natural products; however, the underlying mechanism remains controversial. Through a combination of ^{1}H NMR, solvent isotope effect (SIE) analyses, and mutagenesis applied to two bifunctional dehydratase/enoyl isomerases (DH/EIs), a "His-solo" monofunctional EI, and an engineered "Asp-solo" monofunctional EI, we uncovered a unified catalytic mechanism, highlighting the pivotal role of Asp-H_2O in tuning the ratio of DH and EI activities. This mechanism not only deciphers the catalytic basis of these enzymes but also provides a comprehensive framework for understanding their evolutionary trajectory from DHs to DH/EIs and ultimately to EIs.

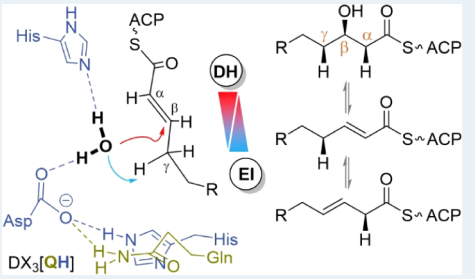

KEYWORDS: *enoyl isomerase, dehydratase, mechanism, polyketide synthase, fatty acid synthesis*

INTRODUCTION

Enzymes have evolved to catalyze diverse chemical reactions essential for life. While understanding how they function offers valuable mechanistic insights, it often fails to explain their evolutionary constraints and thus guide rational engineering. Dehydration (DH) and enoyl isomerization (EI) are critical steps in fatty acid and polyketide biosynthesis, governing product saturation patterns. FabA exemplifies a bifunctional DH/EI enzyme, catalyzing the thermodynamically disfavored and kinetically challenging α,β- to β,γ-double bond isomerization (Scheme 1a), critical in the membrane unsaturated fatty acid biosynthesis.[1,2] Its functional architecture also serves as a prototype for understanding more complex type I polyketide synthases (PKSs). For instance, the bacillaene PKS incorporates two putative DH/EI domains and one dedicated EI domain to assemble its characteristic β,γ-triene system.[3,4]

The catalytic mechanisms of DH/EIs and related monofunctional EIs have been debated since the 1970s.[5] One prevailing theory proposes a catalytic dyad consisting of histidine (His in HX_8P motif) and aspartic acid (Asp in DX_3[QH] motif) which act in concert for deprotonation/reprotonation during the reversible double-bond migration reactions (Scheme 1b).[6−9] In contrast, an alternative hypothesis suggests that His alone acts as the "one-base" involved in the intramolecular hydrogen transfer between Cα and Cγ (Scheme 1c), particularly given the natural occurrence of His-solo EIs and the fact that Asp is predominantly deprotonated at physiological pH (7−8),[10] rendering it unlikely to function as an acid.[2,11−15] However, mechanistic studies consistently demonstrate that mutation of Asp in DH/EIs abolished both DH and EI activities,[6,9,16,17] implicating undiscovered mechanisms. Intriguingly, an evolutionary analysis suggests that Asp-to-Asn substitution represents a critical transition (Figure S1). The crystal structure of a PKS_EI revealed that Asn mimics Asp by hydrogen-bonding H_2O via its amide carbonyl group,[3] implying that subtle variation at this position drove the functional divergence from monofunctional DHs to bifunctional DH/EIs, and ultimately to monofunctional EIs (Scheme 1d).

To resolve this mechanistic controversy and derive evolution-informed engineering principles, we investigated two highly efficient DH/EIs (CoeA_DH and FabA), one His-solo EI (PksEI14),[3] and one engineered Asp-solo EI (CoeA_DH H949F) through extensive kinetic and NMR experiments combined with directed mutagenesis.

RESULTS AND DISCUSSION

Catalytic Mechanism of CoeA_DH. PKS_DHs serve as a reservoir of potential DH/EIs, but they often exhibit low *in vitro* activity, severely limiting their functional characterization.[3,15,18−21] In a genome mining effort targeting DH/EIs, we cloned and expressed multiple candidate DHs predicted by antiSMASH.[22] Using two chemically synthesized substrate surrogates, **1** and **2** (Figures 1a,b and S2−S9), we identified CoeA_DH (SCO6827_PKS_DH.1)[23,24] whose EI activity was significantly higher than that of previously reported EIs[3,9,15] while the DH activity was even 3 orders of magnitude greater (Figure 1c,d).

Received: August 4, 2025
Revised: August 13, 2025
Accepted: August 18, 2025

https://doi.org/10.1021/acscatal.5c05457
ACS Catal. 2025, 15, 15649−15656

Scheme 1. Enoyl Isomerase (EI) and Dehydratase (DH)-Catalyzed Reactions[a]

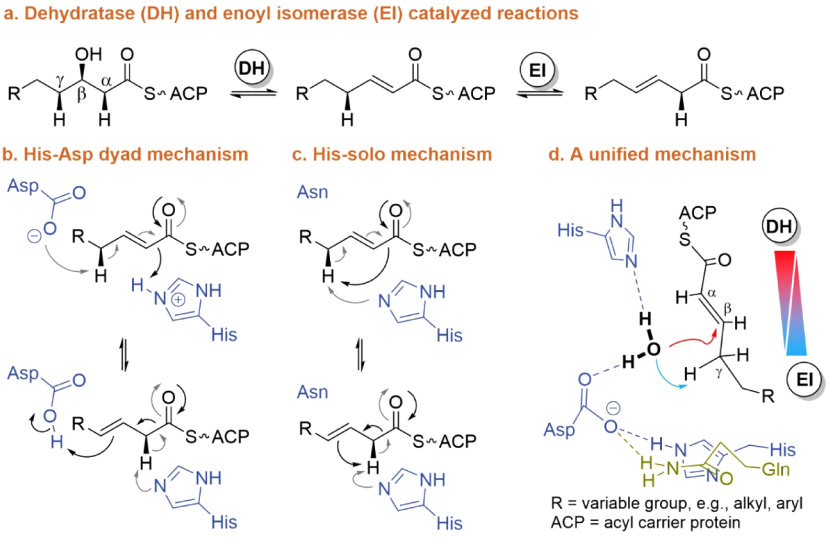

[a]Proposed catalytic mechanisms. (a) Reaction paths of α,β-dehydration by DHs and α,β- to β,γ-double bond migration by EIs. (b,c) Previously proposed EI mechanisms involving either a His-Asp dyad or His alone. (d) Unified mechanism from this study: Asp-H_2O performs either a nucleophilic attack of Cβ for the hydration reaction (red arrow) or mediates Cγ chemistry (abstracts Hγ and initiates double-bond migration), while His facilitates Cα proton transfer. The geometry of Asp-H_2O tunes the DH/EI activity ratio.

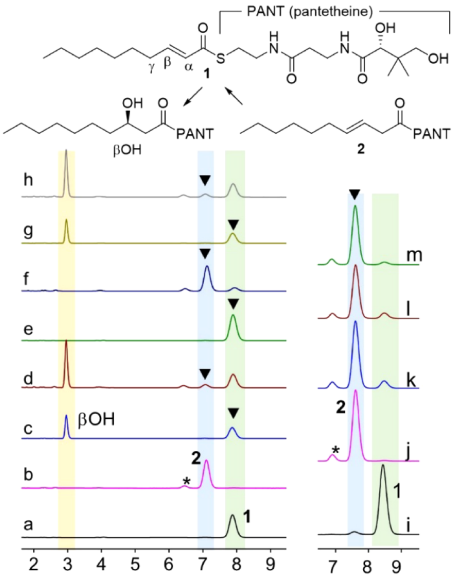

Figure 1. HPLC analysis of *in vitro* reactions. (Top) Structures of synthesized substrates **1** and **2**, with arrows indicating monitored reaction directions (despite the known reversibility of **2**↔**1**↔βOH). (Bottom) HPLC traces for various *in vitro* reactions. (**a,b**) Standards **1** and **2**; (**c,d**) CoeA_DH wild-type: at 10 nM with **1** reached equilibrium, and at 10 μM showed near-complete consumption of **2**; (**e,f**) CoeA_DH H949F mutant: inactive with **1** and reduced activity with **2**; (**g,h**) CoeA_DH H1122Q maintained wild-type reactivities with **1** and **2**; (**i,j**) repeated standards **1** and **2**; (**k**−**m**) PksEI14 wild-type and its mutants S183A and S183G at 200 μM with **2**, showing wild-type to reduced activities. The black triangle (▼) indicates the substrate used, and the asterisk (*) denotes an impurity.

EI reactions primarily involve proton transfer, and thus D_2O-buffered reactions were commonly conducted for isotope exchange experiments.[11−14] But this approach presents two challenges: the background hydrogen/deuterium exchange (HDX) and the solvent isotope effect (SIE), leading to ambiguous results, particularly for EIs and DH/EIs with low activity.[3,9,15] The high activity of CoeA_DH offered an opportunity; by combining NMR spectroscopy (to capture snapshots) with kinetic analysis (to monitor reaction dynamics), we aimed to delineate the complete trajectory of proton transfer.

We first confirmed negligible background HDX at Cα of **2** over a 4-h period (Figure S10), ensuring that all observed HDX within this time frame was enzyme-catalyzed. Scaled-up reactions terminated at 10 min and 2 h, respectively, followed by NMR analysis, revealed rapid HDX at Cα of substrate **2** (Figure 2b ii,iii, *dt*→*dd* peak at 5.45 ppm) and slower deuteration at Cγ of product **1** (*dd* peaks at 6.20 and 6.85 ppm), demonstrating that Cγ reprotonation is the rate-limiting step. The observed large SIE ($v_{0,H_2O}/v_{0,D_2O}$ = 5.3 ± 1.4, Table 1a and Figure S11) further confirms that this step involves D−O bond breaking, with D_2O serving as the exclusive deuterium source. This contrasts with the intramolecular transfer model, where His-D^+ would directly protonate Cγ without solvent participation (Figure 2a).

The course of the α,β to β,γ isomerization was studied by Schwab et al. in the 1980s based on ^{1}H NMR experiments of FabA-catalyzed reactions, establishing the intramolecular hydrogen transfer mechanism. Their work reported anomalous deuterium enrichment at Cα of the β,γ product, which was initially ascribed to the chemical derivation artifacts.[12,13] Subsequent studies attributed HDX phenomena to nonenzyme processes.[3,15] However, our experimental design excluded these possibilities by using highly efficient DH/EI and direct NMR analysis. The unequivocal detection of deuteration at Cα of product **2** (Figure 2b vi, *dd* peaks at 5.45 ppm), coupled with the observed small SIE ($v_{0,H_2O}/v_{0,D_2O}$ = 1.4 ± 0.1, Table 1b), provides definite evidence that the HDX at Cα is enzyme-catalyzed and extremely fast, rendering the Cγ deprotonation the rate-limiting step. Notably, the reaction direction from **1** to **2** may not be adequate to conclude whether the catalytic base for Cγ deprotonation is bound to the D_2O, His, or His-D_2O relay, as any of their relative catalytic efficiencies for Cγ

https://doi.org/10.1021/acscatal.5c05457
ACS Catal. 2025, 15, 15649−15656

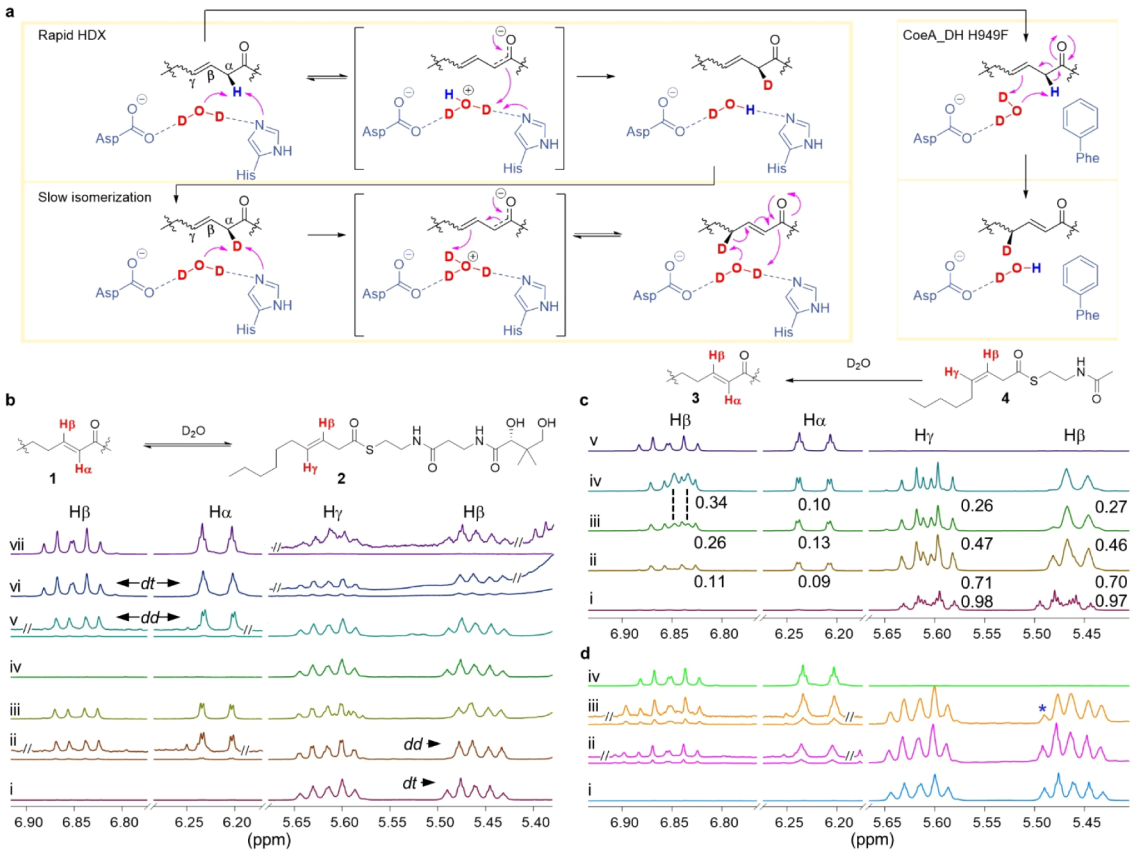

Figure 2. Mechanistic investigation by NMR analysis. (a) Proposed reaction routes for HDX and isomerization, catalyzed by the wild type (left box) and the CoeA_DH H949F mutant (right box). Wave bonds for either variable configurations or substituents are explicitly presented in (b–d). Brackets indicate the hypothesized transition states involving protonated H_3O^+, which are absent in the mutant due to its rate-limiting deprotonation step. (b) CoeA_DH and its mutants: (i) standard **2**; (ii,iii) wild-type with **2** after 10 min and 2-h incubations, respectively; (iv,v) mutants D1118N and H949F with **2**; (vi) wild-type with **1**; and (vii) standard **1**. (c) FabA: (i) standard **4**; (ii–iv) wild-type with **3** for 1, 5, and 12 min, respectively; (v) standard **3**. Vertical dashed lines in (iii,iv) in (c) show the emergence of a doublet, indicating a single proton (Hγ) adjacent to Hβ. Numbers below peaks represent peak integrals; during the reaction, Hβ increases while Hα does not, indicating Hα on **4** is exchanged prior to isomerization. (d) PksEI14: (i) standard **2**; (ii,iii) wild-type from two batches with **2**; and (iv) standard **1**. The asterisk (*) in (iii) denotes the transition from *dt* to *dd* peaks, indicating that Hα on **2** is undergoing exchange. Insets with double slashes (//) show zoomed-in regions. Peak labels *dd* and *dt* indicate doublets of doublets and doublets of triplets, respectively.

Table 1. Measurements of the Solvent Isotope Effect (SIE)[a]

	Reactions	Replicates ($v_{0,H_2O}/v_{0,D_2O}$)			Average ($v_{0,H_2O}/v_{0,D_2O}$)
a	CoeA_DH, 2→1	5.01	4.11	6.83	5.32 ± 1.39
b	CoeA_DH, 1→2	1.32	1.47	1.28	1.37 ± 0.10
c	CoeA_DH H949F, 2→1	1.30	1.23	1.17	1.24 ± 0.07
d	FabA, 4→3	5.48	5.12	6.02	5.54 ± 0.45
e	PksEI14, 2→1	0.81	0.81	0.96	0.86 ± 0.09
f	PksEI14, 2→1	0.64	0.64	0.64	0.64 ± 0.002

[a]Time-course experiments were conducted in H_2O or D_2O buffer to determine initial reaction velocities. All measurements were based on substrate consumption, except for panels **b** and **f**, which were quantified by product formation (Figure S11).

deprotonation may be substantially lower than that of the Cα-activation system.

Targeted mutagenesis studies were applied to His949 and Asp1118 in the active site. HPLC analysis demonstrated that D1118A and D1118N completely lost both DH and EI activities (Figure S12). Unexpectedly, ^{1}H NMR analysis of the D1118N mutant revealed no detectable HDX at the Cα of substrate **2** despite retaining an intact His949 (Figure 2b iv, *dt* peaks at 5.45 ppm). Structural insights from molecular modeling suggest a critical conformational rearrangement: the Asn side chain flips, forming a hydrogen bond with His1122 through its carbonyl group, while its amide NH_2 coordinates the bound D_2O (Figure S13). This substitution attenuates the electrostatic polarization and proton transfer capacity of the bound water, diminishing both its Brønsted acidity and nucleophilicity as a catalyst.

Unexpectedly, the H949F mutant retained ∼10% of the wild-type EI activity but exhibited negligible DH activity (Figures 1e,f and S12). The absence of a meaningful SIE ($v_{0,H_2O}/v_{0,D_2O}$ = 1.2 ± 0.1, Table 1c) suggests that, in the absence of His949, Hα dissociation occurs slowly through keto–enol tautomerization or weak abstraction by Asp-D_2O, followed by rapid reprotonation at Cγ. This kinetic bottleneck prevents the formation of a protonated D_2HO^+ intermediate, thereby suppressing HDX at the Cα (Figure 2a). Together, these findings reveal a shift in the rate-limiting step to Cα deprotonation—a marked contrast to the wild type where Cγ reprotonation dominates kinetics. Remarkably, this Asp-solo active site configuration represents the first instance of functional isolation of EI activity from a native DH/EI and

https://doi.org/10.1021/acscatal.5c05457
ACS Catal. 2025, 15, 15649–15656

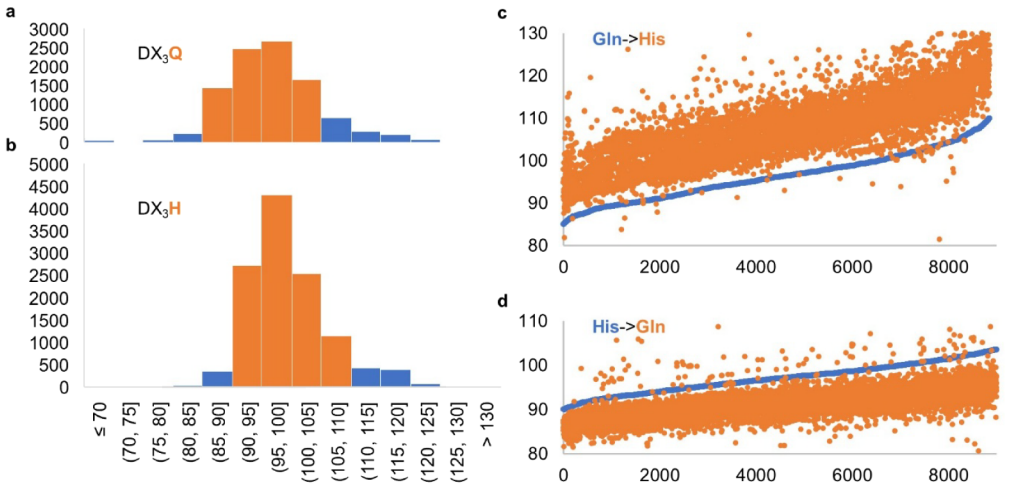

Figure 3. Angle distribution and mutational effects. (a,b) Histograms showing the angle distribution between the Asp carboxylate plane and His imidazole ring in wild-type enzymes, with most values clustered between 85 and 110°. The *x*-axis shows the angle (°) and the *y*-axis indicates the number of DH domains analyzed. (c,d) Scatter plots comparing angle changes in Gln↔His mutants. Blue markers represent wild-type angles (sorted ascendingly), while orange markers show angles after mutation, demonstrating an average ∼10° shift upon residue substitution. The *x*-axis denotes the number of DHs analyzed, and the *y*-axis shows the angle (°).

completes the missing link in the spectrum of catalytic configurations.

Revisiting FabA and PksEI14 toward a Unified Mechanism. Building on the mechanistic insights from CoeA_DH, we hypothesize that FabA, the prototype of DH/EIs, might employ a similar catalytic mechanism. To test this, we conducted extensive NMR experiments based on a prior time-course experiment (Figure S14) using synthesized substrates **3** and **4** (Figures S6−S9).[2] Surprisingly, we observed instant completion of exchange at the first Hα, followed by gradual exchange at the second Hα of **4** (Figure 2c, progressively simplified peaks at 5.45 ppm and complicated peaks at 6.85 ppm). Concomitantly, the product was deuterated at Cγ (Figure 2c ii−iv, *dd* peaks at 6.22 ppm and *dd* complex peaks at 6.85 ppm). Kinetic validation through SIE ($v_{0,H_2O}/v_{0,D_2O}$ = 5.5 ± 0.5, Table 1d) confirmed FabA's higher activity than CoeA_DH. Moreover, these results aligned closely with observations from Bloch's lab, where an unexplained but consistent isotope loss slightly exceeding one Hα was reported.[11] Our findings now clarified this phenomenon as serial hydrogen exchange, revealing that FabA can access and exchange both Hα (Figure S13). This effectively demonstrates an epimerase-like activity, a remarkable feature given its rarity in nonepimerase domains, although it has occasionally been inferred from indirect observations.[25−28] It is worth noting that in computational simulations, the catalytic His was assumed capable of reaching Cγ, whereas the cross-linking experiments only indicated activities restricted to Cα and Cβ.[29,30] Perhaps, the disparity of pK_a values of Hα and Hγ forces DH/EIs to use a H_2O relay, even though Cγ is sterically accessible.

Finally, we revisited PksEI14, the only studied His-solo EI,[3] for which the reaction condition was reported as an enzyme/substrate ratio of 0.46 mM:1 mM with incubation for 36 h. However, the ^{1}H NMR result showed complete HDX at substrate Cα but no deuterium incorporation into product Cγ, contradicting the intramolecular hydrogen transfer mechanism and neither consistent with our proposed model. A plausible explanation is that enzyme-bound H_2O is more resistant to exchange, serving as the sole proton source for Cγ reprotonation in this nearly single-turnover reaction. The crystal structure of PksEI14 (PDB entry 4U3V) revealed that, despite the absence of Gln or His from the DX$_3$[**QH**] motif, Asn maintains an appropriate orientation via hydrogen bonding to a mediator H_2O (H_2O*med*), which is further positioned by two hydrogen bonds from backbone carbonyls and one from Ser-OH (Figure S13). This H_2O*med*-Asn-H_2O*cat* network stabilizes bound H_2O*cat*, implying a mechanism in PksEI14 similar to those in CoeA_DH and FabA.

Furthermore, the crystal structure of PksEI14 reveals a substrate-binding tunnel capable of accommodating approximately a C10-length substrate, although longer substrates are likely required given its role at the late stage of a giant PKS assembly line.[3,7] We cloned and expressed wild-type PksEI14 along with its cognate ACP. Activity assays using chemically synthesized dec-3-enoyl-ACP (Figures S15−S18) revealed moderate catalytic efficiency (Figure S19). Subsequent testing with analog **2** showed reduced activity but still markedly improved over the previously used hex-3-enoyl-*S*-pantetheine.[3] In an initial experiment, the D_2O buffer-exchanged enzyme showed no detectable deuterium incorporation into either substrate **2** or product **1** after a 3-h incubation (Figure 2d i, standard *dt* peaks at 5.45 ppm). But surprisingly, when buffer exchange began at the Ni column purification step, significant HDX was observed on substrate **2** (Figure 2d ii, *dt* peaks at 5.45 ppm transforming to *dd* peaks) with an efficiency between that of the CoeA_DH wild type and the H949F mutant. In contrast, deuterium incorporation at Cγ of product **1** was barely detectable (Figure 2d ii, *dt* peaks at 6.22 and 6.85 ppm), indicating a distinct condition for Cγ reprotonation. The bound H_2O may remain partially replaced by D_2O, leading to a preferential use of H_2O for Cγ reprotonation. Alternatively, complete replacement by D_2O could severely inhibit the reprotonation reaction; in this case, HDX at Cα generates HDO, which promotes Cγ reprotonation. The latter hypothesis aligns with the observed inverse SIE in PksEI14 ($v_{0,H_2O}/v_{0,D_2O}$ = 0.86 ± 0.09 for substrate consumption and 0.64 ± 0.002 for product generation, Table 1e,f), suggesting that the stabilized HD_2O^+ may enhance the otherwise slow Cγ

https://doi.org/10.1021/acscatal.5c05457
ACS Catal. 2025, 15, 15649−15656

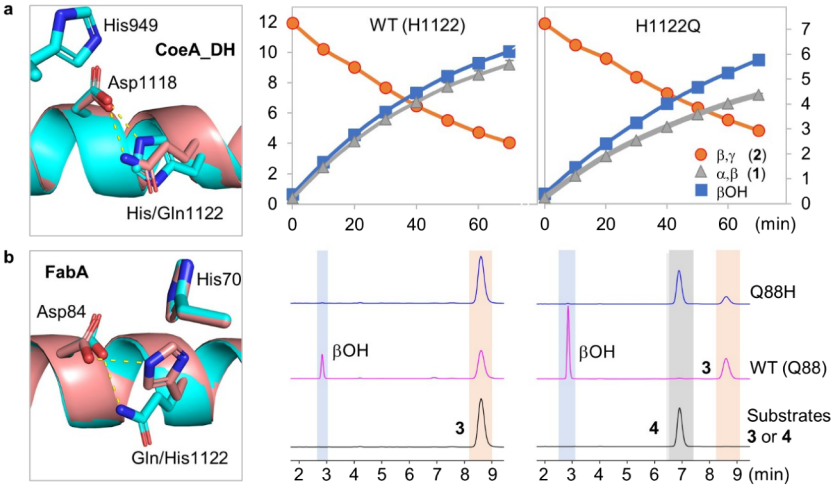

Figure 4. Effects of swapping Gln and His in the motif DX_3[QH]. (a) CoeA_DH and (b) FabA. All models for the wild types and mutants were predicted by AlphaFold3[32] (FabA is precisely aligned with PDB 4b0i.[16] In (a), progress curves for WT and H1122Q reacting with **2** are presented, with peak areas corresponding to the three forms (α,β, β,γ, and βOH). In (b), HPLC traces for FabA WT and Q88H mutant reacting with **3** or **4** are displayed.

reprotonation step.[31] To probe the role of H_2O*med*, S183-[GAVIF] mutants were constructed, but only S183[GA] were solubly expressed and exhibited slightly reduced activities (Figure 1l,m), highlighting the important role of H_2O*med* hard-coded in EIs.

Taken together, our results support a unified mechanism for all three types of EIs (Scheme 1d), where the Asp/Asn-H_2O plays a central role in Cγ deprotonation/reprotonation, while His facilitates those for Cα.

Implication of the Origin of the EI Activity. Beyond mechanistic insights, systematic molecular modeling shows that the Asp-H_2O plane adopts an 85−110° range relative to the His imidazole ring, with the DX_3[QH] motif's Gln/His residue fine-tuning this angle by ∼10° (Figure 3). Experimental testing demonstrated that this geometric control can potentially dictate catalytic outcomes: the CoeA_DH H1122Q mutant increases the DH/EI ratio, while FabA Q88H reduces it to become an apparently specialized EI (Figure 4). This subtle (<10°) angular variation—controlled by the conserved but chemically distinct Gln/His in the DX_3[QH] motif—translates to functional consequences that have long been unexplained.

The spatial positioning of Asp-H_2O acts as a tunable switch that modulates the DH-to-EI activity ratio, enabling a continuous evolutionary trajectory from dedicated DHs to bifunctional DH/EIs and ultimately to specialized EIs. The conservation of this mechanism across fatty acid and polyketide biosynthesis suggests that it may represent a fundamental design principle in nature's toolkit for metabolic innovation.

CONCLUSION

This work establishes a unified mechanism for DH/EIs, His-solo EIs, and Asp-solo EIs, in which Asp/Asn-H_2O orchestrates Cγ chemistry, with His assisting in Cα activation. Small angular changes in the Asp-H_2O geometry tuned by the DX_3[QH] motif shift the ratio of DH and EI activities, outlining a continuous evolutionary path from DHs to DH/EIs and EIs. These findings resolve a decades-long mechanistic debate and provide a structural basis for engineering double-bond-modifying enzymes across fatty acid and polyketide pathways.

MATERIALS AND METHODS

Bacterial Strains, Culture Conditions, and General Remarks. All *Escherichia coli* strains were cultured in Luria−Bertani broth (LB) at 37 °C, supplemented with 50 μg/mL of kanamycin when needed. *E. coli* DH5α was used for cloning and BL21(DE3) for induced protein expression. DNA polymerase was purchased from Vazyme, restriction enzymes were purchased from New England Biolabs (NEB), and competent cells were purchased from Tsingke. Chemicals were ordered from Innochem, Mreda, Meryer, and Macklin.

Plasmid Construction and Protein Expression. All expression plasmids for wild-type proteins were constructed using Gibson Assembly, and the mutant plasmids were constructed using KLD (a homemade mixture of kinase, ligase, and *Dpn*I). DNA fragments were PCR-amplified using 2× Phanta Flash Master Mix and then assembled to a predigested N-His tag backbone (pET28a/*Bam*HI+*Hin*dIII) and transformed into DH5α competent cells. Extracted plasmids were analyzed by sequencing, with the correct constructs transformed into BL21(DE3). Protein expression was induced with 0.1 mM of isopropyl β-D-1-thiogalactopyranoside (IPTG) at OD_{600} 0.6, 20 °C, 200 rpm, overnight. Protein purification was carried out by using Ni-NTA His-tag affinity chromatography.

Synthesis of Compounds 1−4. To 4 mL of H_2O were added *D*-pantethine syrup (1 mmol) and DTT (1 mmol), heated to 50 °C, and stirred for 2 h. The mixture was lyophilized and dissolved in 8 mL of DCM (dichloromethane), yielding a solution of PANT (*R*-pantetheine) at 1 mmol/4 mL. To 5 mL of DCM while stirring were added PANT (1 mmol), carboxylic acid (1 mmol), and DMAP (4-dimethylaminopyridine, 0.1 mmol), followed by EDC (3-(ethyliminomethyleneamino)-*N*,*N*-dimethylpropan-1-amine, 1.1 mmol). The reaction mixture was stirred at room temperature for 30 min and checked by TLC (thin-layer chromatography) or HPLC. The reaction mixture was dried and then purified by silica gel chromatography, and the product was eluted using a mixture of petroleum ether/ethyl acetate/acetone. Fractions containing

https://doi.org/10.1021/acscatal.5c05457
ACS Catal. 2025, 15, 15649−15656

the target product, typically eluted with acetyl acetate:acetone = 1:1 to 2:1, were pooled and dried under vacuum and dissolved in DMSO.

HPLC and HRMS Analyses. HPLC analysis was performed on a SHIMADZU Nexera XR equipped with a diode-array detection (DAD) detector and an analytical column ShimNex WP C18-S (4.6 × 100 mm, 5 μm) at a flow rate of 1.0 mL/min. Wavelengths were set to 235 and 260 nm. Solvent A was water with 0.1% TFA (trifluoroacetic acid), and Solvent B was acetonitrile with 0.1% TFA. Isocratic programs were used: 44% B for 10 min or 55% B for 5 min. For liquid chromatography−mass spectrometry (HRMS) analysis, ESI positive ion mode Waters Xevo G2 XS QToF (Manchester, UK) was used, equipped with an ACQUITY UPLC BEH C18 column (130 Å, 1.7 μm, 2.1 mm × 100 mm).

***In Vitro* Reactions-General Components.** Tris-HCl, pH 7.0, 50 mM; NaCl, 10 mM (200 mM for PksEI14 and its mutants); substrates dissolved in DMSO, 0.5−1.0 mM; enzymes stored in Tris-HCl/NaCl buffer with 40% glycerol. For reactions in D_2O, Tris-HCl/NaCl solution was lyophilized and redissolved in D_2O and repeated three times. Enzymes were concentrated and diluted serially in equal volumes of buffer (80% glycerol and 20% D_2O) to make enzyme stocks, and substrates were directly diluted to DMSO-*d*6 as stocks. Note that the second batch of PksEI14 was eluted from the Ni column by D_2O-dissolved elution buffer and subsequently treated and stored as described above.

Time-Course Experiments. Total volume, 200 μL; reactions incubated in vials at room temperature; autosampling per 10 min; 10 μL per injection; total of 15 injections. Reaction components: CoeA_DH, 0.5 μM with β,γ (**2**), 0.5 mM; FabA, 1 μM with β,γ (**4**), 1 mM. HPLC method, isocratic 44% for 10 min. Triplicates were conducted.

Reactions for Measuring Solvent Isotope Effects (SIE). Reaction mixtures were similar to those used in the time-course experiments described above. Changes were made as follows: CoeA_DH 1 μM, H949F 10 μM, FabA 0.5 μM, PksEI14 200 μM for isomerization from **2** to **1** or **4** to **3**; and CoeA_DH 2.5 μM for **1** to **2**. HPLC methods, isocratic 44% B for 10 min. Paired reactions in H_2O and D_2O were autosampled into HPLC, alternatively, for 6 injections. Triplicates were conducted.

Reactions for NMR Experiments. Negative control: 1.5 mL of β,γ (**2**, 10 mM, ∼6.5 mg, in *d*6-DMSO) was added to 15 mL of D_2O buffer, mixed, and incubated at 30 °C. An aliquot of 5 mL was removed at 2, 3, and 4.5 h and mixed with 1 mL of 0.2 N DCl (D_2O-diluted HCl). The compound was recovered and dissolved in *d*6-DMSO for ^{1}H NMR analysis. CoeA_DH (stock 5 mM, 40% glycerol, 10% D_2O) 400 μL was added to 17.6 mL of D_2O buffer, equilibrated for 5 min, and then mixed with 2 mL of (**2** or **1**, 10 mM, ∼8.6 mg, in d6-DMSO). Two reactions were set up, incubated for 10 min and 2 h, respectively (incubated for 2 h only for reaction **1** to **2**) and then mixed with 3 mL of 0.2 N HCl. The compounds were recovered and dissolved in *d*6-DMSO for ^{1}H, ^{13}C NMR, COSY, and HSQC analyses. FabA (stock 2.7 mM, 40% glycerol, 10% D_2O) 48 μL was added to 11.652 mL of D_2O buffer, equilibrated for 5 min, and then mixed with 1.3 mL of β,γ (**4**, 25 mM, ∼8.36 mg, in *d*6-DMSO). Three reactions were set up, incubated for 1, 5, and 12 min, respectively, and then mixed with 3 mL of 0.2 N DCl. The compounds were recovered and dissolved in *d*6-DMSO for ^{1}H, ^{13}C NMR, COSY, and HSQC analyses. PksEI14 (stock 2 mM, 40% glycerol, 10% D_2O) 2 mL was added to 16 mL of D_2O buffer, equilibrated for 5 min, mixed with 2 mL of (**2**, 10 mM, ∼8.6 mg, in *d*6-DMSO) and then incubated at 30 °C for 3 h. The compound was recovered and dissolved in *d*6-DMSO for ^{1}H NMR analysis. CoeA_DH H949F and D1118N, 10 μM final, were subjected to ^{1}H NMR for analysis of HDX on **2** only.

Protein Modeling and Measurement. To ensure reproducibility, all modeling followed standardized protocols without artificial manipulation. Wild-type and mutant sequences were submitted to either the AlphaFold3 online server (https://alphafoldserver.com/), using the top-ranked *model_0.cif output, or a locally installed ESMfold (https://github.com/facebookresearch/esm), which generates a single structure. All predicted structures were used directly without energy minimization or structural modifications. For the angle calculations, a total of 21,757 bacterial NRPS/PKS DH domains were extracted from the antiSMASH database, with boundaries redefined to cover the full length of the double-hotdog fold. Active DHs containing catalytic His and the [DE]X_3[QH] motif were selected and virtually mutated via Gln/His substitution. All sequences were submitted to ESMfold, and Perl scripts were used to measure both the Asp-carboxylate/His-imidazole angles and distances between the respective Cγ atoms.

■ ASSOCIATED CONTENT

Supporting Information

The Supporting Information is available free of charge at https://pubs.acs.org/doi/10.1021/acscatal.5c05457.

Experimental details, supplementary figures 1−19, and supplementary tables 1−3 (PDF)

■ AUTHOR INFORMATION

Corresponding Authors

Huimin Zhao − *Department of Chemical and Biomolecular Engineering, University of Illinois at Urbana−Champaign, Urbana, Illinois 61801, United States;* orcid.org/0000-0002-9069-6739; Email: zhao5@illinois.edu

Bin Wang − *Department of Microbial Physiological and Metabolic Engineering, State Key Laboratory of Microbial Diversity and Innovative Utilization, Institute of Microbiology, Chinese Academy of Sciences, Beijing 100101, PR China; Beijing Key Laboratory of Genetic Element Biosourcing & Intelligent Design for Biomanufacturing, Beijing 100101, PR China;* orcid.org/0000-0003-3688-332X; Email: wangbin@im.ac.cn

Authors

Bing Chen − *Department of Microbial Physiological and Metabolic Engineering, State Key Laboratory of Microbial Diversity and Innovative Utilization, Institute of Microbiology, Chinese Academy of Sciences, Beijing 100101, PR China; University of Chinese Academy of Sciences, Beijing 100101, PR China*

Jinwei Ren − *State Key Laboratory of Mycology, State Key Laboratory of Microbial Diversity and Innovative Utilization, Institute of Microbiology, Chinese Academy of Sciences, Beijing 100101, PR China*

Complete contact information is available at: https://pubs.acs.org/10.1021/acscatal.5c05457

Author Contributions

[#]B.C. and J.R. contributed equally. The manuscript was written through contributions of all authors. All authors have given approval to the final version of the manuscript.

Notes

The authors declare no competing financial interest.

■ ACKNOWLEDGMENTS

This work was supported by the National Key Research and Development Program of China (2022YFC2303100), the National Natural Science Foundation of China (32270052), and the Beijing Municipal Science & Technology Project (Z241100007724009) to B.W., and partly by grant AI144967 to H.Z. from the US National Institutes of Health (NIH). We thank Erwei Li and Li Wang at the Institute of Microbiology, CAS, for LC-MS and HRMS data acquisition and analyses.

■ ABBREVIATIONS

DH, dehydratase; EI, enoyl isomerase; ACP, acyl carrier protein; PANT, pantetheine; HPLC, high-performance liquid chromatography; HRMS, high resolution mass spectrometry

■ REFERENCES

(1) Wang, H.; Cronan, J. E. Functional replacement of the FabA and FabB proteins of Escherichia coli fatty acid synthesis by *Enterococcus faecalis* FabZ and FabF homologues. *J. Biol. Chem.* **2004**, *279* (33), 34489−34495.

(2) Bloch, K. 15 β-hydroxydecanoyl thioester dehydrase. In *The Enzymes*; Boyer, P. D., Ed.; Academic Press, 1971; Vol. *5*, pp. 441−464.

(3) Gay, D. C.; Spear, P. J.; Keatinge-Clay, A. T. A double-hotdog with a new trick: Structure and mechanism of the *trans*-acyltransferase polyketide synthase enoyl-isomerase. *ACS Chem. Biol.* **2014**, *9* (10), 2374−2381.

(4) Moldenhauer, J.; Gotz, D. C.; Albert, C. R.; Bischof, S. K.; Schneider, K.; Sussmuth, R. D.; Engeser, M.; Gross, H.; Bringmann, G.; Piel, J. The final steps of bacillaene biosynthesis in *Bacillus amyloliquefaciens* FZB42: Direct evidence for β,γ dehydration by a *trans*-acyltransferase polyketide synthase. *Angew. Chem., Int. Ed.* **2010**, *49* (8), 1465−1467.

(5) Labonte, J. W.; Townsend, C. A. Active site comparisons and catalytic mechanisms of the hot dog superfamily. *Chem. Rev.* **2013**, *113* (3), 2182−2204.

(6) Leesong, M.; Henderson, B. S.; Gillig, J. R.; Schwab, J. M.; Smith, J. L. Structure of a dehydratase-isomerase from the bacterial pathway for biosynthesis of unsaturated fatty acids: Two catalytic activities in one active site. *Structure* **1996**, *4* (3), 253−264.

(7) Kusebauch, B.; Busch, B.; Scherlach, K.; Roth, M.; Hertweck, C. Functionally distinct modules operate two consecutive α,β→β,γ double-bond shifts in the rhizoxin polyketide assembly line. *Angew. Chem., Int. Ed.* **2010**, *49* (8), 1460−1464.

(8) Lohr, F.; Jenniches, I.; Frizler, M.; Meehan, M. J.; Sylvester, M.; Schmitz, A.; Gütschow, M.; Dorrestein, P. C.; König, G. M.; Schäberle, T. F. α,β→β,γ-double bond migration in corallopyronin A biosynthesis. *Chem. Sci.* **2013**, *4* (11), 4175−4180.

(9) Dodge, G. J.; Ronnow, D.; Taylor, R. E.; Smith, J. L. Molecular basis for olefin rearrangement in the gephyronic acid polyketide synthase. *ACS Chem. Biol.* **2018**, *13* (9), 2699−2707.

(10) Pahari, S.; Sun, L.; Alexov, E. PKAD: A database of experimentally measured pKa values of ionizable groups in proteins. *Database* **2019**, *2019*, baz024.

(11) Rando, R. R.; Bloch, K. Mechanism of action of β-hydroxydecanoyl thioester dehydrase. *J. Biol. Chem.* **1968**, *243* (21), 5627−5634.

(12) Schwab, J. M.; Habib, A.; Klassen, J. B. A thorough study of the stereochemical consequences of the hydration/dehydration reaction catalyzed by β-hydroxydecanoyl thioester dehydrase. *J. Am. Chem. Soc.* **1986**, *108* (17), 5304−5308.

(13) Schwab, J. M.; Klassen, J. B. Steric course of the allylic rearrangement catalyzed by β-hydroxydecanoylthioester dehydrase. Mechanistic implications. *J. Am. Chem. Soc.* **1984**, *106* (23), 7217−7227.

(14) Sedgwick, B.; Morris, C.; French, S. J. Stereochemical course of dehydration catalysed by the yeast fatty acid synthetase. *Chem. Commun.* **1978**, *5*, 193−194.

(15) Berkhan, G.; Merten, C.; Holec, C.; Hahn, F. The interplay between a multifunctional dehydratase domain and a C-methyltransferase effects olefin shift in ambruticin biosynthesis. *Angew. Chem., Int. Ed.* **2016**, *55* (43), 13589−13592.

(16) Moynié, L.; Leckie, S. M.; McMahon, S. A.; Duthie, F. G.; Koehnke, A.; Taylor, J. W.; Alphey, M. S.; Brenk, R.; Smith, A. D.; Naismith, J. H. Structural insights into the mechanism and inhibition of the β-hydroxydecanoyl-acyl carrier protein dehydratase from *Pseudomonas aeruginosa*. *J. Mol. Biol.* **2013**, *425* (2), 365−377.

(17) Lu, Y.-J.; White, S. W.; Rock, C. O. Domain swapping between *Enterococcus faecalis* FabN and FabZ proteins localizes the structural determinants for isomerase activity. *J. Biol. Chem.* **2005**, *280* (34), 30342−30348.

(18) Xie, X.; Cane, D. E. pH-Rate profiles establish that polyketide synthase dehydratase domains utilize a single-base mechanism. *Org. Biomol. Chem.* **2018**, *16* (47), 9165−9170.

(19) Li, Y.; Dodge, G. J.; Fiers, W. D.; Fecik, R. A.; Smith, J. L.; Aldrich, C. C. Functional characterization of a dehydratase domain from the pikromycin polyketide synthase. *J. Am. Chem. Soc.* **2015**, *137* (22), 7003−7006.

(20) Fiers, W. D.; Dodge, G. J.; Sherman, D. H.; Smith, J. L.; Aldrich, C. C. Vinylogous dehydration by a polyketide dehydratase domain in curacin biosynthesis. *J. Am. Chem. Soc.* **2016**, *138* (49), 16024−16036.

(21) Fiers, W. D.; Dodge, G. J.; Li, Y.; Smith, J. L.; Fecik, R. A.; Aldrich, C. C. Tylosin polyketide synthase module 3: Stereospecificity, stereoselectivity and steady-state kinetic analysis of β-processing domains via diffusible, synthetic substrates. *Chem. Sci.* **2015**, *6* (8), 5027−5033.

(22) Blin, K.; Shaw, S.; Kloosterman, A. M.; Charlop-Powers, Z.; van Wezel, G. P.; Medema, M. H.; Weber, T. antiSMASH 6.0: Improving cluster detection and comparison capabilities. *Nucleic Acids Res.* **2021**, *49* (W1), W29−W35.

(23) Wang, B.; Guo, F.; Huang, C.; Zhao, H. Unraveling the iterative type I polyketide synthases hidden in *Streptomyces*. *Proc. Natl. Acad. Sci. U. S. A.* **2020**, *117* (15), 8449−8454.

(24) Hoshino, S.; Ijichi, S.; Asamizu, S.; Onaka, H. Insights into arsenic secondary metabolism in actinomycetes from the structure and biosynthesis of bisenarsan. *J. Am. Chem. Soc.* **2023**, *145* (32), 17863−17871.

(25) Xie, X.; Garg, A.; Khosla, C.; Cane, D. E. Elucidation of the cryptic methyl group epimerase activity of dehydratase domains from modular polyketide synthases using a tandem modules epimerase assay. *J. Am. Chem. Soc.* **2017**, *139* (28), 9507−9510.

(26) You, Y. O.; Khosla, C.; Cane, D. E. Stereochemistry of reductions catalyzed by methyl-epimerizing ketoreductase domains of polyketide synthases. *J. Am. Chem. Soc.* **2013**, *135* (20), 7406−7409.

(27) Keatinge-Clay, A. T. A tylosin ketoreductase reveals how chirality is determined in polyketides. *Chem. Biol.* **2007**, *14* (8), 898−908.

(28) Holzbaur, I. E.; Ranganathan, A.; Thomas, I. P.; Kearney, D. J. A.; Reather, J. A.; Rudd, B. A. M.; Staunton, J.; Leadlay, P. F. Molecular basis of Celmer's rules: Role of the ketosynthase domain in epimerisation and demonstration that ketoreductase domains can have altered product specificity with unnatural substrates. *Chem. Biol.* **2001**, *8* (4), 329−340.

(29) Nguyen, C.; Haushalter, R. W.; Lee, D. J.; Markwick, P. R. L.; Bruegger, J.; Caldara-Festin, G.; Finzel, K.; Jackson, D. R.; Ishikawa, F.; O'Dowd, B.; McCammon, J. A.; Opella, S. J.; Tsai, S.-C.; Burkart,

https://doi.org/10.1021/acscatal.5c05457
ACS Catal. 2025, 15, 15649−15656

M. D. Trapping the dynamic acyl carrier protein in fatty acid biosynthesis. *Nature* **2014**, *505* (7483), 427−431.
(30) Liu, L.; Yu, Q.; Zhang, H.; Tao, W.; Wang, R.; Bai, L.; Zhao, Y.-L.; Shi, T. Theoretical study on substrate recognition and catalytic mechanisms of gephyronic acid dehydratase DH1. *Catal. Sci. Technol.* **2021**, *11* (6), 2155−2166.
(31) Fernandez, P. L.; Murkin, A. S. Inverse solvent isotope effects in enzyme-catalyzed reactions. *Molecules* **2020**, *25* (8), 1933.
(32) Abramson, J.; Adler, J.; Dunger, J.; Evans, R.; Green, T.; Pritzel, A.; Ronneberger, O.; Willmore, L.; Ballard, A. J.; Bambrick, J.; Bodenstein, S. W.; Evans, D. A.; Hung, C.-C.; O'Neill, M.; Reiman, D.; Tunyasuvunakool, K.; Wu, Z.; Žemgulytė, A.; Arvaniti, E.; Beattie, C.; Bertolli, O.; Bridgland, A.; Cherepanov, A.; Congreve, M.; Cowen-Rivers, A. I.; Cowie, A.; Figurnov, M.; Fuchs, F. B.; Gladman, H.; Jain, R.; Khan, Y. A.; Low, C. M. R.; Perlin, K.; Potapenko, A.; Savy, P.; Singh, S.; Stecula, A.; Thillaisundaram, A.; Tong, C.; Yakneen, S.; Zhong, E. D.; Zielinski, M.; Žídek, A.; Bapst, V.; Kohli, P.; Jaderberg, M.; Hassabis, D.; Jumper, J. M. Accurate structure prediction of biomolecular interactions with AlphaFold 3. *Nature* **2024**, *630* (8016), 493−500.

https://doi.org/10.1021/acscatal.5c05457
ACS Catal. 2025, 15, 15649−15656